Phys. Rev. 120, 300 (1960).
[28]A. Frodesen, O. Skjeggestad, R. Moore, and S. Reucroft, Nucl. Phys. B10, 307 (1969).
[29]A. Firestone, *Experimental Meson Spectroscopy*, edited by C. Baltay and A. Rosenfeld (Columbia Univ. Press, New York, 1970), p. 229.
[30]H. Ring, Ph.D. thesis, University of Michigan, 1970 (unpublished).

PHYSICAL REVIEW D VOLUME 9, NUMBER 1 1 JANUARY 1974

Resonance production in $\bar{p}p \to \pi^+\pi^+\pi^-\pi^-\pi^0$ at 1.6 to 2.2 GeV/c *

R. W. Green,† J. W. Chapman, J. Davidson, J. Lys,‡ and B. P. Roe
The University of Michigan, Ann Arbor, Michigan 48104
(Received 26 March 1973)

The reaction $\bar{p}p \to \pi^+\pi^+\pi^-\pi^-\pi^0$ has been studied at six incident antiproton momenta (1.63, 1.77, 1.83, 1.88, 1.95, and 2.20 GeV/c). The data were taken from a 150 000-picture exposure in the MURA-ANL hydrogen bubble chamber. After examining ambiguities with other final states, a low contamination sample of 12 357 events distributed nearly evenly over the six energies was obtained. Cross sections were determined at each energy. The properties of ρ^0, $\rho^\pm$, ω^0, and η^0 mesons produced in this reaction are discussed; evidence for production of the B meson is presented. The A_2, f, and g mesons are seen, but are not examined in detail. The cross sections of resonance channels are examined using the maximum-likelihood method, with a likelihood function based on Breit-Wigner amplitudes and meson-decay matrix elements. Particular attention is paid to the stability of the results as the detailed form of the fitting functions is varied. The reaction is dominated by the production of the ρ^0, $\rho^\pm$, and ω^0 mesons, with cross sections of about 50%, 50%, and 20% of the five-pion cross section, respectively. The largest channel is found to be $\rho^0\rho^\pm\pi^\mp$, accounting for over one third of the five-pion events. Cross sections of all resonance channels are examined as a function of energy. The resonance-channel cross sections are compared to the cross sections determined in experiments at other energies. Qualitative features are found to be consistent between experiments. The cross sections show fluctuations between experiments which are larger than statistically expected.

I. INTRODUCTION

The MURA 30-in. hydrogen bubble chamber at ANL was exposed to a beam of antiprotons at six momenta between 1.6 and 2.2 GeV/c. Approximately 53 000 four-charged-prong interactions were measured on film-plane digitizers and analyzed with the TVGP-SQUAW system. This paper reports on $\bar{p}p$ annihilations into $\pi^+\pi^+\pi^-\pi^-\pi^0$. Four-particle states are discussed in a companion paper.[1] ω-ρ interference will not be discussed here since it was reported on in an earlier publication.[2]

Events which fit the one-constraint hypothesis $\bar{p}p \to \pi^+\pi^+\pi^-\pi^-\pi^0$ are often also consistent with other final states—four pions, six pions, or kaonic final states. The method used to determine the five-pion cross sections at the separate energies and to produce a low-contamination sample of 12 357 events for further analysis is discussed in Sec. II.

The $2\pi^+2\pi^-\pi^0$ state is dominated by the production of intermediate resonance states, mainly ρ, ω, and f mesons. The properties of these and other resonance states are examined in Sec. III. The relative amounts of resonance channels are determined by a maximum-likelihood method; the results are examined and compared with other experiments in Sec. IV.

II. EVENT SAMPLE AND CROSS SECTIONS

A. Four-prong measurement

The average point count per track view was initially set at eight. In order to increase the rate of measuring, the last 80% of the measurements was made with exactly four points per track view. When the events were constrained to the one-constraint five-pion hypothesis, a fit to the effective mass of $\pi^+\pi^-\pi^0$ combinations in the ω^0-meson region found an ω^0 Breit-Wigner width of 32.7 ± 1.5 MeV/c^2 for the four-point-per-track events compared to 29.3 ± 2.0 MeV/c^2 for the many-point-per-track events. Since the ω^0 width is due largely to mass resolution error, it would appear that, for constrained events, the accuracies of the two measuring methods are about the same.

Approximately 2000 events which initially failed the processing sequence were remeasured in order to check for biases in failing events. The percent-

ages of events giving successful fits to each of the possible final states were the same within errors for both remeasured events and events which passed the processing sequence initially. Duplicate events were removed and a sample of 44 890 properly measured, unique events remained.

The four-prong topological cross sections are presented in Table I and Fig. 1(a). The determination of these topological cross sections is given in detail elsewhere.[1,3]

B. Cross sections for $\bar{p}p \to \pi^+\pi^+\pi^-\pi^-\pi^0$

The five-pion cross section can be obtained from

$$\sigma(\text{five pions}) = \frac{N(\text{five pions})}{N(\text{four prongs})}\sigma(\text{four prongs}),$$

where N(five pions) is the true number of five-pion events, and N(four prongs) and σ(four prongs) are the number of well-measured four-prong events and the four-prong topological cross sections, respectively, from Table I. The task of obtaining a five-pion cross section is largely that of accounting for events which are ambiguous between the five-pion hypothesis and the other fit hypotheses. The CL (confidence level) distribution for the five-pion hypothesis has a large low-confidence level peak, due to non-five-pion events which fit the five-pion hypothesis. Therefore we eliminate from consideration all events which fit the five-pion hypothesis with a confidence level of less than 1%. In computing the final number of five-pion events, it is then necessary to make a correction for this 1% loss. This particular cut removes the majority of the ambiguous events.

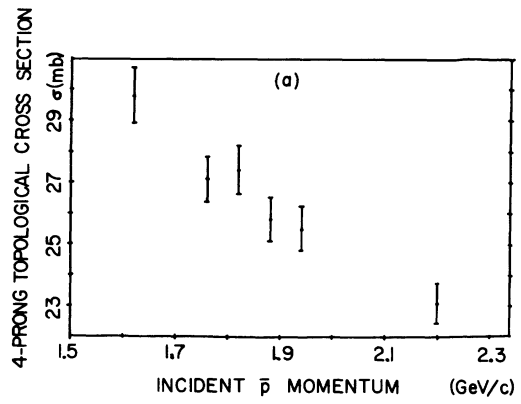

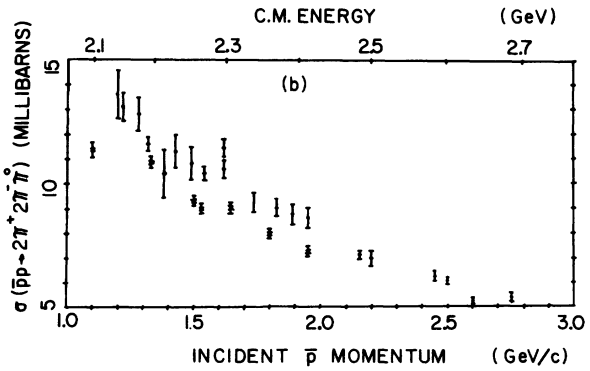

FIG. 1. (a) The four-prong topological cross section as a function of the $\bar{p}$ laboratory momentum. (b) The five-pion cross section as determined from this and other experiments. The data are numerically presented in Table II with references.

In order to check that this confidence level cut does not remove much more than 1% of the true five-pion events, the invariant mass of $\pi^+\pi^-\pi^0$ combinations from events removed by this cut was examined. Any ω^0 mesons observed should be due to five-pion events in the sample. Looking ahead to later sections, we find about 2800 ω^0 mesons to be produced in the sample of events with a confidence level greater than 1%. The resulting plot (not shown) is consistent with having 1% of this number of ω mesons.

Next we consider the cases in which five-pion events with confidence levels greater than 1% are ambiguous with other hypotheses. At the energies of this experiment, ionization measurements provide a very near unique identification of hypotheses ambiguous with five pions and containing at least one different particle assignment. All such ionization-separable fits were appropriately classified. The ambiguities between four- and five-pion fits were resolved by assignment of events to the five-pion category if

$$\frac{\text{confidence level (five-pion)}}{\text{confidence level (four-pion)}} > 4.$$

The error introduced in the five-pion event count by this separation is estimated to be 0^{+60}_{-40} events. The number of events at each momentum after this subtraction were, in order of increasing momenta, 2641, 2922, 2588, 2920, 2773, and 2095.

In order to obtain a quantitative estimate of the contamination of multi-π^0 events in the five-pion

TABLE I. Four-prong-event measurements and cross sections.

Incident $\bar{p}$ momentum (GeV/c)	c.m. energy (MeV)	Four-prong cross section (mb)	Number of events	Events per μb
1.63	2294	29.77 ± 0.82	6990	0.235 ± 0.007
1.77	2347	27.10 ± 0.72	7980	0.294 ± 0.008
1.83	2368	27.38 ± 0.78	7569	0.276 ± 0.008
1.88	2389	25.78 ± 0.70	8057	0.313 ± 0.008
1.95	2410	25.49 ± 0.69	7846	0.308 ± 0.008
2.20	2500	23.05 ± 0.64	6448	0.280 ± 0.007
		total number of events = 44 890		

event sample, a χ^2 fit to the missing mass squared has been made over the region 0.3 to 1.6 $(\mathrm{GeV}/c^2)^2$ of events consistent with multi-π^0 production from which all previous assigned events had been removed. The function used in the fit was a combination of the invariant mass of $\pi^0\pi^0$ from $2\pi^+2\pi^-2\pi^0$ phase space and the invariant mass of $\pi^0\pi^0\pi^0$ from $2\pi^+2\pi^-3\pi^0$ phase space. Since the missing-mass-squared spectrum is due essentially to these multi-π^0 channels, fitting in this manner in the higher-mass region should predict the shape of the low-mass region of the missing-mass-squared spectrum near the π^0 peak. The fit has been done at each momentum. Assuming that four-pion events are sufficiently constrained so as not to include true $2\pi^+2\pi^-2\pi^0$ or $2\pi^+2\pi^-3\pi^0$ events, we conclude that the missing low-mass multi-π^0 events were misidentified as five-pion events. This correction ranged between 100 and 200 events per momentum interval.

We define contamination by

$$c = \frac{N_{K\ \mathrm{fits}} + N_{m\pi 0}}{N_{5\pi} - (N_{K\ \mathrm{fits}} + N_{m\pi^0})},$$

where $N_{5\pi}$ is the number of events in the current five-pion sample, and $N_{K\ \mathrm{fits}}$ and $N_{m\pi^0}$ are the estimated contamination due to unresolved K fits and multi-π^0 events, respectively. The average contamination is $(7.2 \pm 1.0)\%$ for this sample of events.

The five-pion cross sections can now be computed. The results are given in Table II[4-8] and are plotted in Fig. 1(b) along with the results of several other experiments. The errors quoted include the statistical error, estimates of errors in subtraction of contaminants, and the estimate of the four-prong cross section error. The cross-section plot displays two different smoothly falling cross sections. The upper curve, plotted with dots is from the ANL and Michigan experiments in the 30-in. MURA-ANL bubble chamber and from the Liverpool experiments in CERN bubble chambers. The lower curve plotted with crosses is from the Brookhaven and Michigan State experiments in the 31-in. BNL (Ref. 4) bubble chamber. While there is a 10% to 20% normalization difference in the two curves, there are no 2- or 3-mb enhancements in the five-pion cross section corresponding to the $\bar{p}p$ total cross-section enhancements in this energy region.[9]

C. Final event sample

For further analysis, it was desirable to reduce the $(7.2 \pm 1.0)\%$ contamination level of the five-pion sample. To achieve a lower contamination sample, the confidence level for the five-pion hypothesis was required to be greater than 15% for the four-point-per-track events and greater than 5% for the many-point-per-track events. This sample will be used for the remainder of this article. The new confidence-level cuts reduced the total five-pion sample from 15 939 events to 12 367 events. This new sample should have a reduced contamination particularly from multi-π^0 events, although a quantitative estimate of the contamination is difficult to make.

TABLE II. Five-pion cross sections in the 1.1- to 2.9-GeV/c incident $\bar{p}$ momentum range.

Experimenter (reference)	Incident $\bar{p}$ momentum (GeV/c)	Five-pion cross section (mb)
BNL (Ref. 4)	1.1	11.4 ± 0.3
	1.33	10.9 ± 0.2
	1.53	9.0 ± 0.2
Liverpool (Ref. 16)	1.2	13.6 ± 1.0
ANL (Ref. 6)	1.22	13.1 ± 0.6
	1.28	12.8 ± 0.7
	1.32	11.6 ± 0.3
	1.38	10.4 ± 1.0
	1.43	11.3 ± 0.7
	1.49	10.8 ± 0.7
	1.54	10.4 ± 0.3
	1.62	11.4 ± 0.4
Michigan State Univ. (Ref. 7)	1.50	9.3 ± 0.2
	1.65	9.1 ± 0.2
	1.80	8.4 ± 0.2
	1.95	7.3 ± 0.2
	2.15	7.2 ± 0.3
	2.45	6.3 ± 0.2
	2.60	5.2 ± 0.2
	2.75	5.4 ± 0.2
	2.90	4.7 ± 0.2
Univ. of Michigan (this report)	1.63	10.6 ± 0.4
	1.77	9.3 ± 0.4
	1.83	9.0 ± 0.4
	1.88	8.8 ± 0.4
	1.95	8.7 ± 0.4
	2.20	7.0 ± 0.3
Liverpool (Ref. 8)	2.5	6.0 ± 0.1

As a check on the consistency of this new sample, the center-of-momentum angle between the antiproton and the neutral pion has been examined. Since the proton and antiproton are charge conjugates, one would expect that the neutral pion would be symmetric with respect to the proton and antiproton. Of the 12 367 events in this final sample, we would expect 6183 ± 56 events with $\cos\theta$ greater than zero. The data show 6009 events with $\cos\theta$ greater than zero, which is about three standard deviations from the predicted number. This could indicate contamination from other channels. However, the effect is small—about 2%. Comparison of the momentum spectrum of the charged and neutral pions also is consistent with the contamination is being small.

III. PROPERTIES OF RESONANCES

For invariant mass spectra the following mass bands are employed:

ρ^0: 0.680 to 0.840 GeV/c^2,

$\rho^\pm$: 0.660 to 0.820 GeV/c^2,

ω^0: 0.740 to 0.820 GeV/c^2,

f^0: 1.180 to 1.320 GeV/c^2,

The invariant mass plots in this section are taken from the combined data from the middle four momentum sets, since most-likelihood fits were performed for these combined momenta. All other plots in this section are taken from the combined data of all six momentum sets.

Several invariant mass spectra are shown in Figs. 2–5 as solid-line histograms. Unless otherwise stated, the Monte Carlo predictions of the resonance-likelihood Fit (4), to be described in Sec. IV, are given by the "+"'s on the same figures.

A. The ρ meson

Figures 2(a) and 2(b) show clearly the production of the ρ meson in its neutral and charged states in the 750-MeV/c^2 region.

The ω^0 meson is kinematically reflected into the $\pi^+\pi^-$ and $\pi^\pm\pi^0$ effective-mass spectra because the ω^0's mass, about 780 MeV/c^2, forces the mass of any two of the ω^0's three decay pions to fall between 280 and 640 MeV/c^2. The background around the ρ region contains these events. Therefore, all Breit-Wigner fits for the ρ meson were made to the two-pion mass spectra of events in which no $\pi^+\pi^-\pi^0$ effective mass falls in the ω^0 mass band given by 743 to 823 MeV/c^2. The background for the fits was determined by generating Monte Carlo phase-space events and rejecting any event with a $\pi^+\pi^-\pi^0$ effective mass in the ω^0 band.

Fits were performed over the 370-900 MeV/c^2 region of the $\pi^+\pi^-$ and $\pi^\pm\pi^0$ mass spectra, using the combined data from all six momentum sets; the function used in the fits was

$$F(M_{\pi\pi}) = AB(M_{\pi\pi})[1 + Cf_{\mathrm{BW}}(M_{\pi\pi})],$$

where

$M_{\pi\pi}$ = two-pion effective mass,

A, C = constants determined by the fit,

B = background function described above,

and

f_{BW} = resonance amplitude function (Breit-Wigner).

We find that the constant-width relativistic Breit-Wigner function fits the data well. Of the several background and resonance functions tried, the Breit-Wigner distribution with a mass-dependent width suggested by angular momentum barrier considerations gives a significantly poorer fit to the data. The ρ mass and width found in the constant-width fit were 750 ± 3 MeV/c^2 and 168 ± 5 MeV/c^2, respectively, for the neutral ρ, and 751 ± 2 MeV/c^2 and 157 ± 5 MeV/c^2 for the charged ρ. These mass and (constant) width values were used in the maximum-likelihood fitting to be described later on.

B. The ω meson

The invariant-mass-squared distribution for $\pi^+\pi^-\pi^0$ combinations has been fitted in the 0.4 to 0.9 (GeV/c^2)^2 region with a simple Breit-Wigner function and a quartic polynomial in mass squared [Fig. 4(a)]. The fitted mass value of 781.7 ± 0.7 MeV/c^2 is in only fair agreement with the current best value[10] of 783.86 ± 0.30 MeV/c^2. The error quoted for our ω^0 mass reflects only the statistical error and not any systematic errors. From the

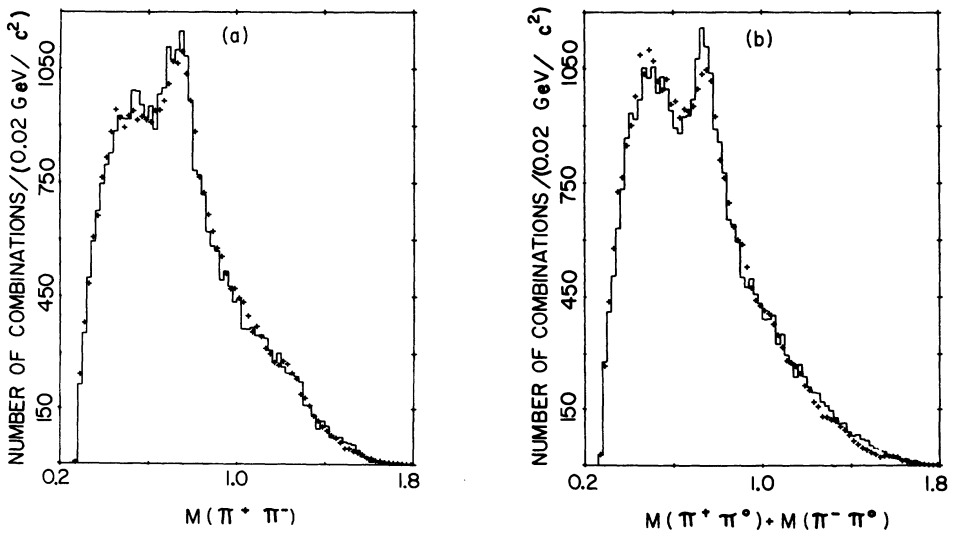

FIG. 2. Invariant masses—middle four momenta (GeV/c^2) (4 combinations/event). (a) $\pi^+\pi^-$ pairs; (b) $\pi^\pm\pi^0$ pairs.

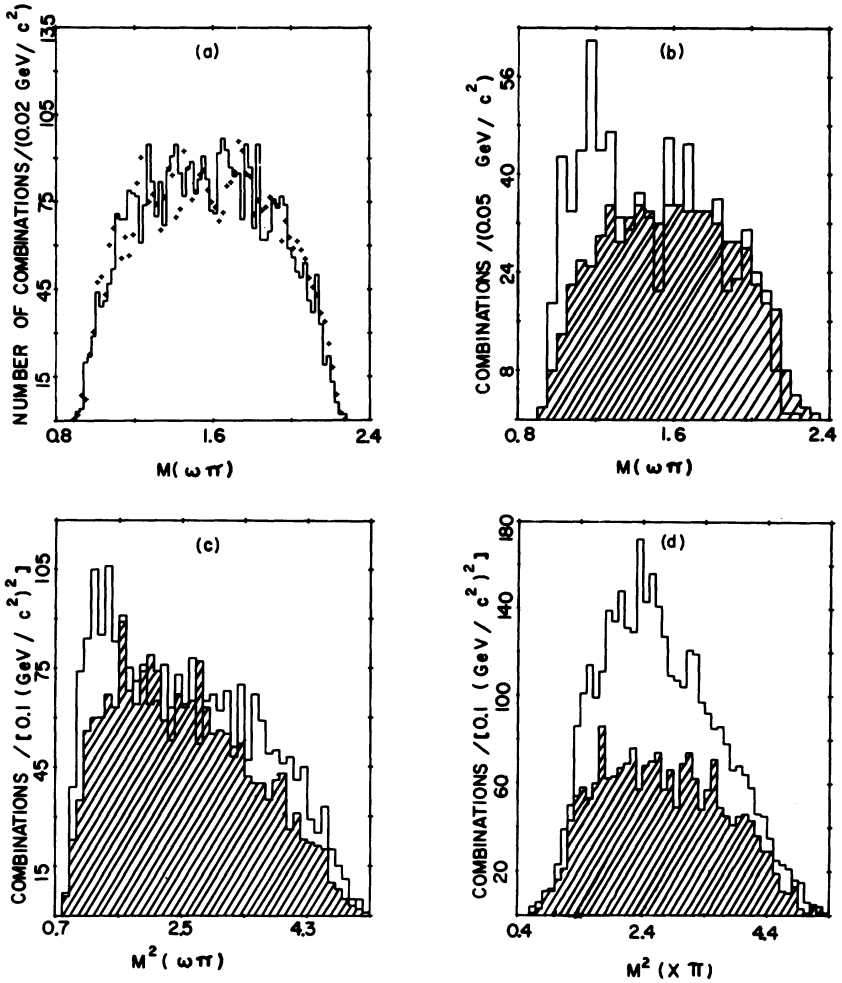

FIG. 3. Invariant masses—middle four momenta. (a) The invariant mass (GeV/c^2) of $\omega^0\pi^\pm$ combinations. (b) The invariant mass (GeV/c^2) of $\omega^0\pi^\pm$ pairs with the cosine of the $\omega^0\pi^\pm$ c.m. production angle >0.85 (unshaded) and <0.85 (shaded; normalized; see text). (c) The invariant mass squared [(GeV/c^2)^2] of $\omega^0\pi^\pm$ combinations for which the absolute value of the cosine of the ω^0 c.m. production angle is ≥ 0.6 (unshaded) or <0.6 (shaded; normalized; see text). (d) The invariant mass squared [(GeV/c^2)^2] of $X^0\pi^\pm$ combinations for which the absolute value of the cosine of the X^0 c.m. production angle is ≥ 0.6 (shaded) or <0.6 (unshaded).

fitted width of 31.7 ± 1.5 MeV/c^2 we have found a 19.8 ± 1.7 MeV/c^2 experimental resolution using the 11.46 ± 0.84 MeV/c^2 best value natural width.[10] This separation was made under the assumption that the experimental width was approximately represented by a Breit-Wigner shape.

C. The η meson

The η^0 meson is seen in the invariant mass spectrum of $\pi^+\pi^-\pi^0$ combinations in the 550 MeV/c^2 region. The mass and width of the η^0 are given, respectively, as 548.82 ± 0.56 MeV/c^2 and 0.0027 ± 0.0007 MeV/c^2.[10] The apparent width of the η^0 in our data reflects the measuring resolution.

The invariant-mass-squared distribution for $\pi^+\pi^-\pi^0$ combinations has been fitted in the 0.23 to 0.42 (GeV/c^2)^2 region with a polynomial background function and a simple Breit-Wigner function. The fitted mass value of 548.7 ± 1.2 MeV/c^2 is in excellent agreement with the current best value given above. The observed width of 15.8 ± 3.5 MeV/c^2 agrees well with the Breit-Wigner mass resolution of 19.8 ± 1.7 MeV/c^2 computed in the ω^0 fitting subsection B. For future maximum-likelihood fits we use the fitted values of the η^0 and ω^0 mass and width obtained above.

D. The B meson

The B meson, with a mass of 1235 MeV/c^2, decays mainly via $B^\pm \to \omega^0\pi^\pm$. The B was first reported in π^+p interactions at 3.5 GeV/c, and has since been reported in π^+p and π^-p interactions at several energies from 3.5 to 11.2 GeV/c and in $\bar{p}p$ interactions. In $\bar{p}p$ at rest,[11] the B meson is

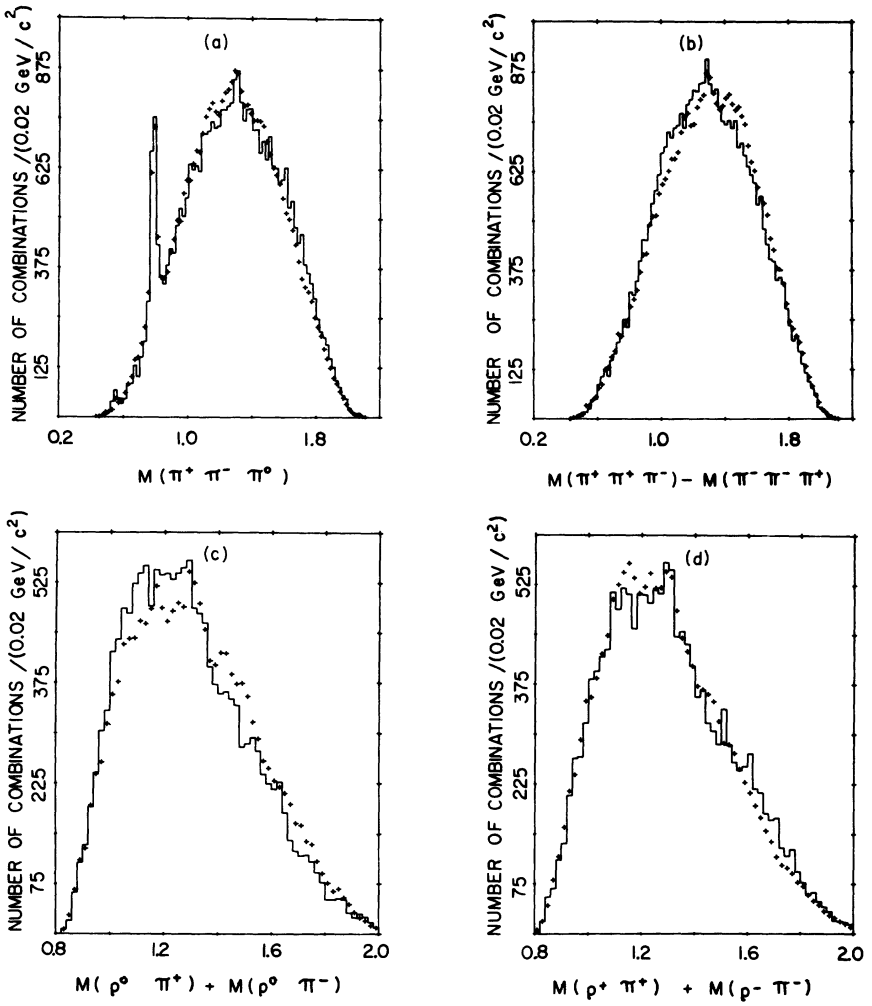

FIG. 4. Invariant masses—middle four momenta (GeV/c^2). (a) $\pi^+\pi^-\pi^0$ combinations (4/event); (b) $\pi^+\pi^+\pi^-$ and $\pi^+\pi^-\pi^-$ combinations (4/event); (c) $\rho^0\pi^+$ and $\rho^0\pi^-$ combinations; (d) $\rho^+\pi^-$ and $\rho^-\pi^+$ combinations.

produced in about 4% of the five-pion events and accounts for nearly 20% of the ω mesons produced. For $\bar{p}$ interactions above 1 GeV/c, there is some disagreement in the literature. Kalbfleisch[4] reports that the $B^{\pm}\pi^{\mp}$ channel accounts for (3–4)% of the five-pion channel over the incident $\bar{p}$ momentum range 1.1–1.5 GeV/c. However, Donald[16] reports an upper limit for the $B^{\pm}\pi^{\mp}$ channel of only 1% of the five-pion channel at 1.2-GeV/c $\bar{p}p$ interactions.

Figure 3(a), the invariant mass of $\omega^0\pi^{\pm}$ combinations in our experiment, shows at most a slight enhancement in the 1200-MeV/c^2 region. In fact, using Monte Carlo events weighted by maximum-likelihood Fit (3) (Sec. IV A 3) assuming no B meson, we see that the number of events above the predicted Monte Carlo curve for $\omega^0\pi^{\pm}$ combinations was found to be 0 ± 25 in the B region, for the combined data from the middle four momentum sets. However, this likclihood fit, based on a phase-space and Breit-Wigner likelihood function, cannot conclusively rule out B-meson production.

The B signal was enhanced in the following way. The $\omega\pi^{\pm}$ combinations were plotted against θ, the center-of-momentum angle between the $\omega\pi^{\pm}$ and the nucleon of like charge. A control region for $\pi^+\pi^-\pi^0$ mass surrounding the ω^0 was defined in a similar manner. A cluster near zero degrees at an $\omega\pi^{\pm}$ mass of ~1150 MeV/c^2 is observed for the $\omega^0\pi^{\pm}$ events, but not in the control region defined as 3π mass 620–720 and 840–940 MeV/c^2.

To further illustrate the $\omega^0\pi^{\pm}$ signal in the zero-angle region, a histogram of the $\omega\pi^{\pm}$ mass for $\cos\theta_{\omega\pi} > 0.85$ is shown in Fig. 3(b). A clear enhancement in the 1200-MeV/c^2 region is observed.

To estimate the background, the $\omega^0\pi^{\pm}$ masses for $\cos\theta_{\omega\pi} < 0.85$ have been normalized such that the number of events in the 1500–1900 MeV/c^2 mass region equaled the number in the $\cos\theta_{\omega\pi}$

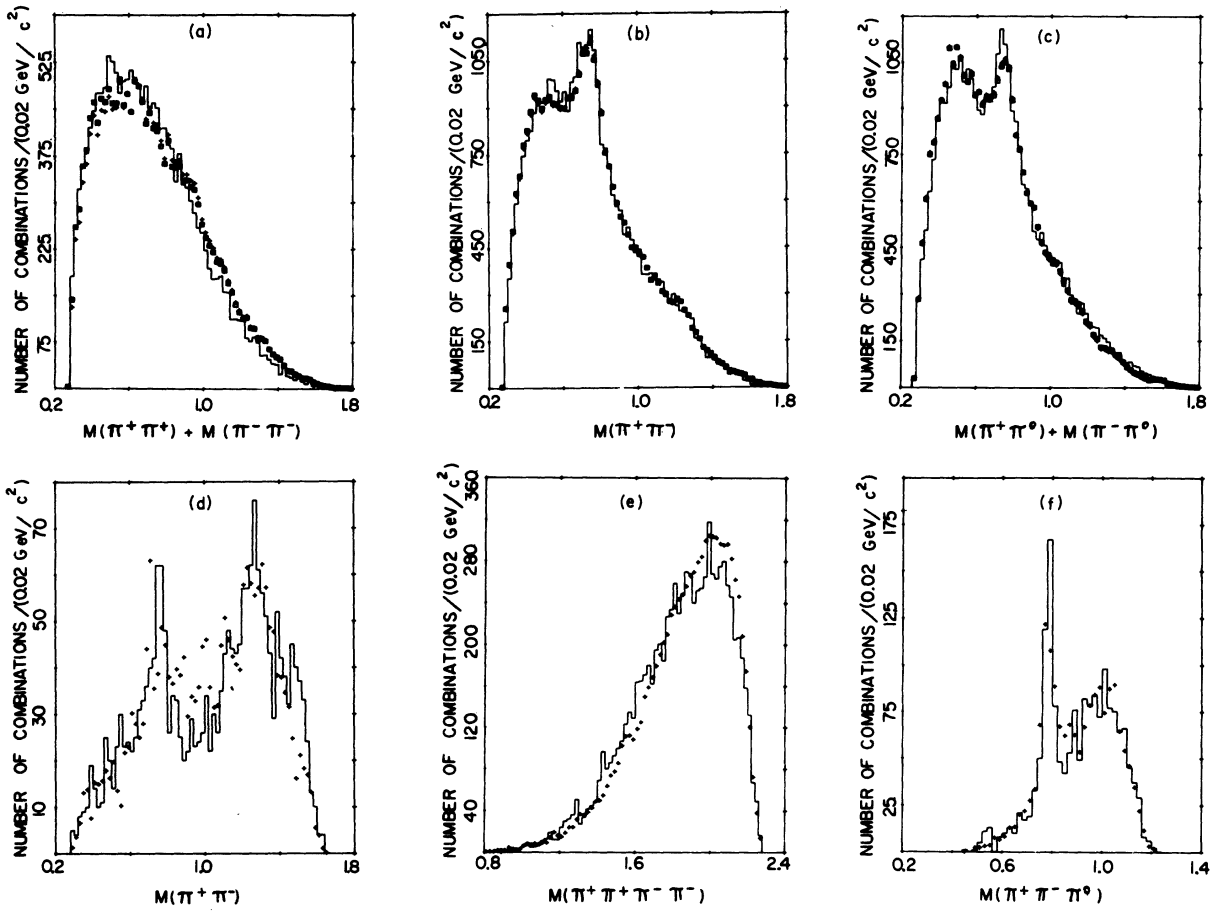

FIG. 5. Invariant masses—middle four momenta (GeV/c^2) compared with the predictions of Likelihood Fit 2 (+) and Fit 3 (□) for (a), (b), (c) and with Fit 4 (+) for (d), (e), (f). (a) $\pi^{\pm}\pi^{\pm}$ combinations; (b) $\pi^+\pi^-$ combinations; (c) $\pi^{\pm}\pi^0$ combinations; (d) $\pi^+\pi^-$ pairs opposite ω^0 mesons; (e) $\pi^+\pi^+\pi^-\pi^-$ combinations (1/event); (f) $\pi^+\pi^-\pi^0$ combinations opposite f^0 mesons.

≥ 0.85 sample in the same mass region. This background estimate is shown by the shaded histogram of Fig. 3(b). For events above the background estimate with effective mass in the region 950–1350 MeV/c^2, the mean value of the mass is found to be 1129 ± 19 MeV/c^2 for 137 mass combinations. The mean mass value is much lower than the observed B-meson mass of 1235 MeV/c^2. However, the error is based only on the statistical uncertainty of subtracting histogram values with $\sqrt{N}$ errors, and does not take into account the uncertainty in the use of the arbitrary background estimate.

Evidence for this enhancement is also seen if the following cut is made. Let θ be the angle between the ω^0 and the antiproton in the reaction center-of-momentum system. Consider two samples: $|\cos\theta| \geq 0.6$ and $|\cos\theta| < 0.6$. For the former, the ω^0 "follows" either the proton or antiproton; for the latter, the ω^0 is more perpendicular to the antiproton direction. In Fig. 3(c), the unshaded histogram presents the effective mass squared of the $\omega^0\pi^{\pm}$ combinations for the $\cos\theta \geq 0.6$ cut; the shaded histogram is the same mass squared for the $\cos\theta < 0.6$ cut, normalized so that the 1.9–2.3 (GeV/c^2)^2 bins in the shaded histogram contain the same number of events as these bins in the unshaded histogram. The normalization was performed over this region, since, if the B meson were produced, one would expect its mass squared to be less than 1.9 (GeV/c^2)^2 and the other $\omega^0\pi^{\pm}$ combination of the event to have a mass squared greater than 2.3 (GeV/c^2)^2. Indeed an enhancement is seen in the 1.2–1.4 (GeV/c^2)^2 region for ω^0 events, where the ω^0 follows the proton or antiproton.

There are 214 events above the background estimate in the mass-squared region 0.8–1.6 (GeV/c^2)^2. This number is fairly consistent with the previous estimate of 137 events, considering the arbitrary nature of the background estimates and the possibility that events were lost by the strict

$\cos\theta_{\omega\pi} \geq 0.85$ selection of the 137-event sample. For the 214 events, the mean mass squared is 1.26 ± 0.22 $(\mathrm{GeV}/c^2)^2$, or a mass of 1122 ± 100 MeV/c^2. Again the error is statistical, and the mass value agrees with the B-meson mass, within errors. The number of events above background in the mass-squared region above 2.3 $(\mathrm{GeV}/c^2)^2$ is 201. This region should contain the reflection of each $\omega^0\pi$ mass in the B region; 201 compares well with the 214 events in the B region.

In Fig. 3(d), the mass squared for the control region $X^0\pi^\pm$ is plotted. The shaded events are events with $|\cos\theta_X| \geq 0.6$, and correspond to the $\omega^0\pi^\pm$ mass-squared plot showing the 1.2–1.4 $(\mathrm{GeV}/c^2)^2$ enhancement. The unshaded histogram is for events with $|\cos\theta_X| < 0.6$. The two histograms were not normalized in any way. There are no obvious mass enhancements.

Thus, an enhancement is seen in the 1100–1200 MeV/c^2 $\omega^0\pi^\pm$ invariant mass region. The enhancement is seen only for $\omega^0\pi^+\pi^-$ events, with very forward $(\omega^0\pi^\pm)$ production angles. Choosing ω^0 mesons following the antiproton or proton produces the same effect. These cuts are necessary since the number of events in the enhancement is small ($\lesssim 220$) compared to the number of $\omega^0\pi^\pm$ combinations (~6300). This analysis does not rule out the possibility that this enhancement is a kinematic effect, but does show consistency with the B meson. By simple background estimates, the size of the enhancement appears to be 140–215 events, or about (1.2–1.8)% of the five-pion events. The amount of B production will be determined by the maximum-likelihood method in Sec. IV A 4 arbitrarily assuming a B-meson mass and width of 1220 MeV/c^2 and 120 MeV/c^2, respectively.

E. Other mesons

The invariant mass plots show evidence for several other resonances, but, due to the poor peak-to-background ratios, it is not possible to accurately examine the masses and widths of these resonances.

In particular, the invariant mass spectrum of all $\pi^+\pi^-$ pairs [Fig. 2(a)] and the invariant mass spectrum of $\pi^+\pi^-$ pairs opposite an ω^0 meson [Fig. 5(d)] exhibit an enhancement in the 1200–1300 MeV/c^2 region—the f^0 meson. This enhancement appears too wide for the f^0 alone, and perhaps suggests the g^0 meson.

The $\pi^+\pi^-\pi^0$, $\pi^\pm\pi^\pm\pi^\mp$, $\rho^0\pi^\pm$, and $\rho^\pm\pi^\mp$ spectra (Fig. 4) all show evidence for the A_2 meson, with a mass of about 1300 MeV/c^2.

Since it is desirable to use the maximum-likelihood method to solve for the production rates of these resonances, the following resonance mass and width values will be used in the likelihood search[10]:

	Mass (MeV/c^2)	Width (MeV/c^2)
f^0	1260	150
g^0	1670	165
A_2^{+-0}	1300	100

F. $\omega\pi\pi$ and $\rho\pi\pi$ events

The center-of-mass angular distributions for events consistent with $\omega^0\pi^+\pi^-$ production were examined. A peak for events with the charged pions going opposite to the direction of the like-charged baryon (not shown) was found in addition to the expected forward peak. The $\omega^0\pi^+\pi^-$ distribution was compared with those for the four-constraint hypothesis[1] $\rho^0\pi^+\pi^-$ and a similar effect was found. The enhancement in both cases was found associated with $\pi^+\pi^-$ events in the f^0 region, i.e., $\omega^0 f^0$ and $\rho^0 f^0$ events. The production angular distributions are quite similar for these two channels and the production mechanisms are probably related. However, no single simple mechanism was found. An s-channel effect is unlikely since $\rho^0 f^0$ requires $I=1$ and $\omega^0 f^0$ requires $I=0$. A simple proton exchange in the t channel appears unlikely since the upper vertex coupling should be nine times stronger for $\bar{p}p \to \rho^0$ than for $\bar{p}p \to \omega^0$, whereas experimentally we find that the $\omega^0 f^0$ channel (610 ± 60 μb) is larger than the $\rho^0 f^0$ channel (350 ± 80 μb) averaged over our energies. The $\sigma(\omega^0 f^0)$ (246 ± 45 μb) was also found to exceed the $\sigma(\rho^0 f^0)$ (198 ± 30 μb) by Fields[5] *et al.* at 2.3 GeV/c.

IV. RESONANCE-CHANNEL CROSS SECTIONS

In Sec. III the properties of resonances found in the five-pion reaction were discussed. We now use a maximum-likelihood fitting method to determine the cross sections for the resonances. The fitting procedure was similar to that used in the four-meson paper.[1]

Throughout this section, the term "percent" refers to "percent of the five-pion cross section." The term "M(mesons)" refers to "the invariant mass of (mesons)."

A. The maximum-likelihood fitting

The four primary fits described in this section are successively more complex attempts at obtaining the resonance channel percentages. A fifth fit, making an arbitrary attempt to include properties of the $\omega^0\pi^+\pi^-$ system in the likelihood function, was made.

Table III presents the resonance percentages and log-likelihood magnitude for the four primary fits to the combined data of the middle four momenta,

TABLE III. Summary of Fits (1)–(4) to combined data from the middle four momenta. Here and in Tables VI–X the different resonant channels are mutually exclusive. Furthermore "all ρ^0" includes ρ^0 from A_2 decay; $\rho^0\rho^0\pi^0$ events are counted twice and similarly for "all $\rho^\pm$."

Channel	Fit (1)	Fit (2)	Fit (3)	Fit (4)
$\rho^0\pi^+\pi^-\pi^0$	14.0	12.8	0.0	0.0
$\rho^0\rho^\pm\pi^\mp$	38.5	39.4	44.1	29.4
$\rho^\pm\pi^+\pi^-\pi^\mp$	7.6	7.2	0.0	0.0
$\rho^0\rho^0\pi^0$	0.7	1.0	2.6	2.3
$\rho^0 f^0\pi^0$	0.5	0.8	1.4	1.5
$f^0\pi^+\pi^-\pi^0$	0.0	0.0	0.0	...
$f^0 f^0\pi^0$	0.0	0.0	0.0	...
$f^0\rho^\pm\pi^\mp$	6.3	6.6	6.3	5.6
$\omega^0\pi^+\pi^-$	6.6	5.6	5.4	8.1
$\omega^0\rho^0$	2.5	2.8	3.1	2.0
$\omega^0 f^0$	6.8	7.1	7.0	6.6
$\omega^0 g^0$	3.1	2.9	3.0	...
$\eta^0\pi^+\pi^-$	0.6	0.5	0.5	...
$A_2^0\pi^+\pi^-$	...	...	...	5.4
$A_2^0\rho^0$	...	...	...	1.7
$A_2^\pm\pi^\mp\pi^0$	...	...	...	1.7
$A_2^\pm\rho^\mp$	...	...	...	4.1
$B^\pm\pi^\mp$	...	...	...	2.0
$2\pi^+2\pi^-\pi^0$	12.6	14.2	26.3	29.3
All ρ^0	56.9	57.8	53.8	45.0
All $\rho^\pm$	52.4	53.2	50.4	46.2
All ω^0	19.0	18.5	18.6	18.7
All $\rho^0\rho^\pm\pi^\mp$	38.5	39.4	44.1	35.2
$\log_{10}L$	545.8	599.4	625.7	638.4

TABLE IV. Monte Carlo χ^2 comparison with experiment.

Invariant mass distribution	χ^2 Fit (1)	Fit (2)	Fit (3)	Fit (4)	Fit (5)	Bins
$\pi^-\pi^-$	228	239	203	209	201	70
$\pi^+\pi^-$	198	164	166	127	129	72
$\pi^+\pi^+$	101	105	86	88	83	65
$\pi^-\pi^0$	177	128	116	113	116	73
$\pi^+\pi^0$	194	185	162	157	163	72
$\pi^+\pi^-\pi^-$	239	217	202	182	189	79
$\pi^+\pi^+\pi^-$	148	131	122	103	105	78
$\pi^-\pi^-\pi^0$	89	85	96	96	93	75
$\pi^+\pi^-\pi^0$	271	289	230	226	227	80
$\pi^+\pi^+\pi^0$	117	123	132	117	127	74
$\pi^+\pi^+\pi^-\pi^-$	190	189	155	141	150	61
$\pi^+\pi^-\pi^-\pi^0$	105	101	99	99	95	64
$\pi^+\pi^+\pi^-\pi^0$	129	132	130	106	116	65
$\pi^+\pi^-\pi^0$ opp ρ^0	155	150	137	117	120	58
$\pi^+\pi^-\pi^0$ opp f^0	55	65	66	69	69	34
$\pi^+\pi^-\pi^0$ opp f^+ [a]	53	54	53	58	49	26
$\pi^+\pi^-$ opp ρ^0	85	83	82	82	80	58
$\pi^+\pi^-$ opp f^0	76	48	49	49	49	31
$\pi^+\pi^-$ opp ω^0	107	116	116	142	126	68
$\pi^+\pi^-$ opp $\rho^\pm$	146	127	126	108	108	59
$\pi^\pm\pi^0$ opp ρ^0	196	194	176	166	172	60
$\pi^\pm\pi^0$ opp f^0	56	47	47	48	46	34
$\omega^0\pi^\pm$	82	88	91	96	95	64
$\rho^0\pi^0$	173	167	140	139	141	58
$f^0\pi^0$	50	37	36	36	36	34
$\rho^0\pi^\pm$	314	310	278	229	238	61
$f^0\pi^\pm$	41	34	33	33	33	36
$\rho^\pm\pi^\mp$	174	167	156	125	118	62
Total	3947	3775	3485	3261	3274	1671

[a] f^+ refers to the $\pi^+\pi^-$ mass region above 1.32 GeV/c^2.

TABLE V. MINOS error analysis of Fit (4).

Channel	Middle four momenta Fit	+error	−error [a]	1.83 GeV/c only Fit	+error	−error [a]
$\rho^0\pi^+\pi^-\pi^0$	0.0	0.8	...	0.0	2.2	...
$\rho^0\rho^\pm\pi^\mp$	29.4	2.3	2.3	29.8	4.4	4.4
$\rho^\pm\pi^+\pi^-\pi^0$	0.0	0.6	...	0.0	3.4	...
$\rho^0\rho^0\pi^0$	2.3	1.2	1.2	0.3	1.8	...
$\rho^0 f^0\pi^0$	1.5	0.9	0.9	3.1	1.9	1.8
$A_2^0\pi^+\pi^-$	5.4	1.2	1.2	2.4	2.4	2.2
$A_2^0\rho^0$	1.7	1.2	1.2	3.7	2.2	2.2
$A_2^\pm\pi^\mp\pi^0$	1.7	1.2	1.2	1.7	2.3	...
$A_2^\pm\rho^\mp$	4.1	1.1	1.1	4.2	2.3	2.2
$f^0\rho^\pm\pi^\mp$	5.7	1.0	1.0	5.9	2.2	2.1
$\omega^0\pi^+\pi^-$	8.1	1.1	1.0	8.0	2.2	2.1
$\omega^0\rho^0$	2.0	0.5	0.5	1.0	1.0	0.9
$\omega^0 f^0$	6.6	0.6	0.6	6.8	1.2	1.2
$B^\pm\pi^\mp$	2.1	0.5	0.5	3.1	1.1	1.1
$2\pi^+2\pi^-\pi^0$	29.3			29.9		

[a] "..." indicates that the channel percentage is consistent with zero.

and Table IV presents the χ^2 comparison of experimental invariant mass distributions and invariant mass distributions resulting from Monte-Carlo-generated events weighted by the likelihood function.

Because the determination of exact statistical errors by the fitting program required a very large amount of computer time, this was performed for only one fit. These errors can then be considered approximate errors for all the other fits. It would be useful for the reader to look ahead to Table V to see the typical statistical error associated with the resonance percentages presented in the following subsections.

1. *The basic fit*

In this likelihood fit, Fit (1), the $\rho^0_\pm$, f^0, g^0, ω^0, and η^0 channels are investigated.

The fourteen channels used are

(i) single-meson channels $\rho^0\pi^+\pi^-\pi^0$, $\rho^\pm\pi^+\pi^-\pi^\mp$, $\omega^0\pi^+\pi^-$, $f^0\pi^+\pi^-\pi^0$, and $\eta^0\pi^+\pi^-$;

(ii) double-meson channels. $\rho^0\rho^\pm\pi^\mp$, $\rho^0\rho^0\pi^0$, $\rho^0 f^0\pi^0$, $\rho^\pm f^0\pi^\mp$, $f^0 f^0\pi^0$, $\omega^0\rho^0$, $\omega^0 f^0$, and $\omega^0 g^0$;

(iii) phase space. $\pi^+\pi^+\pi^-\pi^-\pi^0$.

The matrix elements are an incoherent sum of (products of) Breit-Wigner functions.

The results of the maximum-likelihood fit are given in Table VI in terms of the percentages of the five-pion cross section. The fit was performed separately at each of the six momenta and using combined data from the middle four momenta to enhance our statistics. The center-of-momentum energy spread of these four momenta is only 60 MeV.

Several features of the fit are immediately ob-

TABLE VI. Results of maximum-likelihood Fit (1) in terms of percentages of the five-pion cross section.

	Incident antiproton momentum (GeV/c)						
Channel	1.77, 1.83, 1.88, 1.95	1.63	1.77	1.83	1.88	1.95	2.20
$\rho^0\pi^+\pi^-\pi^0$	14.0	8.7	11.6	9.5	10.4	17.0	26.7
$\rho^0\rho^\pm\pi^\mp$	38.5	47.8	36.2	40.6	42.2	28.2	24.2
$\rho^\pm\pi^+\pi^-\pi^\mp$	7.6	2.1	10.6	6.9	6.7	16.6	16.3
$\rho^0\rho^0\pi^0$	0.7	0.0	5.1	0.1	0.2	2.8	5.3
$\rho^0 f^0\pi^0$	0.5	1.9	0.2	2.4	0.0	2.0	0.2
$f^0\pi^+\pi^-\pi^0$	0.0	0.0	0.0	0.0	0.0	0.0	0.0
$f^0 f^0\pi^0$	0.0	0.6	0.0	0.7	1.6	0.0	0.7
$f^0\rho^\pm\pi^\mp$	6.3	5.0	6.5	5.2	3.9	1.9	8.8
$\omega^0\pi^+\pi^-$	6.6	7.7	4.5	8.9	8.2	5.1	10.6
$\omega^0\rho^0$	2.5	4.2	3.7	0.7	3.1	2.1	1.0
$\omega^0 f^0$	6.8	5.6	6.9	6.9	6.1	6.9	3.4
$\omega^0 g^0$	3.1	6.0	3.4	2.4	3.0	3.3	1.8
$\eta^0\pi^+\pi^-$	0.6	0.8	0.7	0.3	0.5	0.6	0.7
$2\pi^+2\pi^-\pi^0$	12.6	9.1	10.3	14.8	13.6	13.0	0.0
All ρ^0	56.9	62.6	61.9	53.3	56.1	54.9	62.7
All $\rho^\pm$	52.4	54.9	53.3	52.5	52.8	46.7	49.3
All ω^0	19.0	23.5	18.5	18.9	20.4	17.4	16.8
$\log_{10}L$	545.8	164.8	156.8	125.5	152.2	122.1	97.9
Events	8608	2161	2220	2089	2222	2077	1589

TABLE VII. Results of maximum-likelihood Fit (2) in terms of percentages of the five-pion cross section.

	Incident antiproton momentum (GeV/c)						
Channel	1.77, 1.83, 1.88, 1.95	1.63	1.77	1.83	1.88	1.95	2.20
$\rho^0\pi^+\pi^-\pi^0$	12.8	8.8	13.2	1.6	9.0	26.7	28.4
$\rho^0\rho^\pm\pi^\mp$	39.4	48.5	45.1	44.3	43.1	22.3	22.7
$\rho^\pm\pi^+\pi^-\pi^\mp$	7.2	1.7	0.0	2.9	6.3	25.2	17.1
$\rho^0\rho^0\pi^0$	1.0	0.0	1.2	1.5	0.5	1.2	5.0
$\rho^0 f^0\pi^0$	0.8	2.4	0.0	3.4	0.1	2.2	0.0
$f^0\pi^+\pi^-\pi^0$	0.0	0.0	0.0	0.0	0.0	0.0	0.0
$f^0 f^0\pi^0$	0.0	0.0	0.0	0.0	1.6	0.0	0.1
$f^0\rho^\pm\pi^\mp$	6.6	5.7	10.6	5.6	4.6	2.2	9.9
$\omega^0\pi^+\pi^-$	5.6	8.7	3.6	7.3	7.6	3.8	9.7
$\omega^0\rho^0$	2.8	3.9	4.0	1.5	3.4	2.4	1.1
$\omega^0 f^0$	7.1	5.6	7.8	7.0	6.2	7.2	3.4
$\omega^0 g^0$	2.9	4.9	3.0	2.4	2.7	3.4	1.8
$\eta^0\pi^+\pi^-$	0.5	0.8	0.7	0.3	0.4	0.6	0.6
$2\pi^+2\pi^-\pi^0$	14.2	8.8	10.6	22.2	14.3	2.8	0.0
All ρ^0	57.8	63.6	64.7	53.8	56.6	55.9	62.3
All $\rho^\pm$	53.2	56.0	55.7	52.8	54.0	49.7	49.7
All ω^0	18.5	23.1	18.4	18.3	20.0	16.8	15.9
$\log_{10}L$	599.4	181.4	166.9	139.5	168.6	132.0	105.7
Events	8608	2161	2220	2089	2222	2077	1589

vious. The ρ meson, in all three charge states, and the ω^0 meson dominate the five-pion reaction. The $\rho^0\rho^\pm\pi^\mp$ channel is by far the largest channel at around 40%. The charged modes $\rho^0\rho^\pm\pi^\mp$ (about 40%) and $f^0\rho^\pm\pi^\mp$ (about 6%) are much larger than their all-neutral counterparts $\rho^0\rho^0\pi^0$ and $f^0\rho^0\pi^0$, which are in fact consistent with 0%. Though the total ρ-meson percentages are approximately constant as a function of energy, the $\rho^0\rho^\pm\pi^\mp$ channel appears to decrease as energy increases, and the $\rho^0\pi^+\pi^-\pi^0$ and $\rho^\pm\pi^+\pi^-\pi^\mp$ channels increase with energy. Within errors, no other channels exhibit striking energy dependence.

From Table IV, it is seen that the total χ^2 for the 28 experimental histograms (1671 bins) is a poor 3947.

2. *Addition of the ω decay matrix element*

Fit (1) was unable to reproduce well the $\pi^+\pi^-$ and $\pi^\pm\pi^0$ invariant mass spectra in the region below the ρ mesons. The ω^0 meson reflects kinematically into these regions. Fit (2) uses the same likelihood function as Fit (1), but with the addition of a 1^- decay matrix element for the ω^0 meson. The results of Fit (2) are given in Table VII; the fit to the middle four momenta can be compared with Fit (1) in Table III. Note that the fit percentages are, within fitting errors, the same percentages as for Fit (1). However, the log likelihood is significantly increased: for the four-momenta fit, an increase of 53.67, from 545.77 to 599.44.

The improvement in the goodness of fit is also seen in the χ^2 for the Monte Carlo comparison with the experimental mass spectra. From Table IV it is seen that the total χ^2 for 1671 bins has decreased by 172, from 3947 to 3775. In particular, the $\pi^+\pi^-$ and $\pi^\pm\pi^0$ invariant mass spectra are better reproduced in the low-mass region.

3. *Addition of Bose-Einstein correlations*

Throughout Fits (1) and (2), the greatest discrepancy between experimental and Monte Carlo distributions occurs in the $M(\pi^+\pi^+)$ and $M(\pi^-\pi^-)$ spectra. In the experimental spectra, the low masses (under 700 MeV/c^2) appear to be enhanced, and the high masses (above 700 MeV/c^2) decreased, relative to the Monte Carlo likelihood-weighted event spectra. This effect does not appear in the other two-pion mass spectra—$M(\pi^+\pi^-)$ and $M(\pi^\pm\pi^0)$—however. Goldhaber[12] hypothesized that it is necessary, in multi-pion final states, to take into account correlations between pions of like charge due to Bose-Einstein statistics. These correlations take the form of a modification to phase space in which phase-space events are weighted by a factor

$$F = [1 + \exp(-a|\vec{p}_{+1} - \vec{p}_{+2}|^2)] \times [1 + \exp(-a|\vec{p}_{-1} - \vec{p}_{-2}|^2)],$$

$$a = \left(\frac{\lambda}{2.15}\frac{\hbar}{m_\pi c}\right)^2,$$

where $\vec{p}_{+1}$ is the three-momentum of the first positive pion, and so on, and λ is a constant estimated by Goldhaber to be between about 0.5 and 0.75. Events in which the like-charge pions are near to each other ($\vec{p}_1 - \vec{p}_2$ small) and hence have a low effective mass are weighted more heavily by this factor.

TABLE VIII. Results of maximum-likelihood Fit (3) in terms of percentages of the five-pion cross section.

Channel	Incident antiproton momentum (GeV/c) 1.77, 1.83, 1.88, 1.95	1.63	1.77	1.83	1.88	1.95	2.20
$\rho^0\pi^+\pi^-\pi^0$	0.0	0.0	0.0	0.0	0.0	0.7	15.3
$\rho^0\rho^\pm\pi^\mp$	44.1	48.0	45.9	44.4	47.1	33.5	29.3
$\rho^\pm\pi^+\pi^-\pi^-$	0.0	0.0	0.0	0.0	0.0	11.6	8.7
$\rho^0\rho^0\pi^0$	2.6	1.0	3.8	0.8	0.2	5.7	6.9
$\rho^0 f^0\pi^0$	1.4	2.9	0.0	3.4	0.0	3.4	0.0
$f^0\pi^+\pi^-\pi^0$	0.0	0.0	0.0	0.0	0.0	0.0	0.0
$f^0 f^0\pi^0$	0.0	0.0	0.0	0.0	0.6	0.0	0.0
$f^0\rho^\pm\pi^\mp$	6.3	3.9	9.1	5.6	4.8	1.9	10.4
$\omega^0\pi^+\pi^-$	5.4	8.1	3.1	7.6	7.7	3.3	9.4
$\omega^0\rho^0$	3.1	4.2	4.4	1.6	3.6	2.8	1.2
$\omega^0 f^0$	7.0	5.6	7.9	7.0	6.2	7.1	3.3
$\omega^0 g^0$	3.0	5.0	3.1	2.5	2.7	3.5	1.8
$\eta^0\pi^+\pi^-$	0.5	0.8	0.7	0.3	0.4	0.6	0.6
$2\pi^+2\pi^-\pi^0$	26.3	20.4	22.0	26.4	26.4	25.8	12.8
All ρ^0	53.8	57.1	56.8	50.9	51.0	50.7	59.6
All $\rho^\pm$	50.4	51.9	55.0	50.0	52.0	47.0	48.3
All ω^0	18.6	22.9	18.4	18.7	20.1	16.7	15.8
$\log_{10}L$	625.7	187.5	173.3	145.1	176.3	136.5	106.4
Events	8608	2161	2220	2089	2222	2077	1589

Fit (3) incorporates the Bose-Einstein correlation factor with $\lambda = 0.5$. The likelihood function is otherwise the same as in Fit (2). A fit to the middle four momenta leaving λ free obtained $\lambda = 0.48$ with virtually unchanged likelihood and percentages from those shown in Fit (3). $\lambda = 0.4$ or $\lambda = 0.6$ decreases the log likelihood by about 35. The results of Fit (3) are presented in Table VIII and compared with the previous fits in Tables III and IV.

The magnitude of the log likelihood has increased significantly from 599.4 to 625.7. The total ρ^0, $\rho^\pm$, and ω^0 percentages are only slightly changed: The ρ^0 and $\rho^\pm$ have decreased by (3–4)%. The percentages of all processes containing ω^0 or f^0 mesons are unchanged. Indeed, the only significant change is in the manner in which the ρ^0's and $\rho^\pm$'s match up. In Fit (3), compared to the earlier fits, the $\rho^0\pi^+\pi^-\pi^0$ and $\rho^\pm\pi^+\pi^-\pi^\mp$ channels have markedly decreased, and the channel $\rho^0\rho^\pm\pi^\mp$ has increased correspondingly.

From Table IV it is seen that the total χ^2 for the mass spectra has been reduced from Fit (2) to Fit (3) by 290, from 3775 to 3485. As was hoped, the fits to $M(\pi^+\pi^+)$ and $M(\pi^-\pi^-)$ were significantly improved; the predictions of Fits (2) and (3) for the combined $M(\pi^\pm\pi^\pm)$ spectrum are shown in Fig. 5(a). The addition of Bose-Einstein correlations was a step in the right direction, but not a sufficient step. Therefore, the Goldhaber effect appears to be insufficient to explain the $M(\pi^\pm\pi^\pm)$ spectrum in these data. For comparison, the predictions of Fits (2) and (3) for the $M(\pi^+\pi^-)$ and $M(\pi^\pm\pi^0)$ spectra are presented in Figs. 5(b) and 5(c), respectively. The Goldhaber correlations affect these spectra very little.

TABLE IX. Results of maximum-likelihood Fit (4) in terms of percentages of the five-pion cross section.

Channel	Incident antiproton momentum (GeV/c) 1.77, 1.83, 1.88, 1.95	1.63	1.77	1.83	1.88	1.95	2.20
$\rho^0\pi^+\pi^-\pi^0$	0.0	0.0	0.0	0.0	0.0	0.0	0.3
$\rho^0\rho^\pm\pi^\mp$	29.4	32.7	26.6	29.8	34.5	23.1	26.4
$\rho^\pm\pi^+\pi^-\pi^\mp$	0.0	0.0	0.0	0.0	0.0	4.8	0.6
$\rho^0\rho^0\pi^0$	2.3	0.4	3.6	0.3	1.6	4.2	6.6
$\rho^0 f^0\pi^0$	1.5	3.0	0.0	3.1	1.6	2.5	0.0
$A_2^0\pi^+\pi^-$	5.4	1.7	5.4	2.5	5.5	7.1	6.4
$A_2^0\rho^0$	1.7	7.3	3.2	3.7	1.0	0.0	0.0
$A_2^\pm\pi^\mp\pi^0$	1.7	2.9	0.9	1.7	1.2	2.4	8.6
$A_2^\pm\rho^\mp$	4.1	0.2	6.2	4.2	2.1	4.5	0.6
$f^0\rho^\pm\pi^\mp$	5.6	3.2	8.2	5.9	3.9	3.2	10.4
$\omega^0\pi^+\pi^-$	8.1	10.0	6.7	8.0	10.8	6.5	8.8
$\omega^0\rho^0$	2.0	3.4	3.2	1.0	2.5	1.4	0.8
$\omega^0 f^0$	6.6	6.0	7.8	6.8	5.8	6.2	2.9
$B^\pm\pi^\mp$	2.0	3.6	0.9	3.1	1.3	3.0	3.7
$2\pi^+2\pi^-\pi^0$	29.3	25.4	27.2	29.9	28.1	31.0	23.8
All ρ^0	45.0	50.4	47.3	43.8	46.1	42.3	49.6
All $\rho^\pm$	46.2	45.1	49.6	46.1	47.0	42.6	44.4
All ω^0	18.7	23.0	18.6	18.9	20.4	17.1	16.2
All $\rho^0\rho^\pm\pi^\mp$	35.2	40.2	36.0	37.8	37.6	27.8	27.0
$\log_{10}L$	638.5	190.2	177.9	149.9	177.7	139.7	113.9
Events	8608	2161	2220	2089	2222	2077	1589

4. *Addition of A_2 and B mesons*

The last major addition to be made to the likelihood function is two resonances which decay via other resonances, namely, the A_2 and B mesons. The A_2 meson is seen in the neutral mode $A_2^0 \to \rho^\pm\pi^\mp$ and the charged mode $A_2^\pm \to \rho^0\pi^\pm$. The B meson occurs in the charged mode $B^\pm \to \omega^0\pi^\pm$. Fit (4) is essentially the same as Fit (3), but with the addition of these A_2 and B probability amplitudes. In order to restrict the number of parameters to a reasonable number, the $f^0\pi^+\pi^-\pi^0$, $f^0 f^0\pi^0$, $\eta^0\pi^+\pi^-$, and $\omega^0 g^0$ processes were not included in Fit (4).

The results of Fit (4) are given in Table IX and compared with the previous fits in Tables III and IV. There is an improvement in the log likelihood for the fit to the combined data from the middle four momenta from 625.71 to 638.49. The total ω^0 percentage and the individual ω^0 channel percentages remain nearly the same as in Fit (3). The fitted values for the total ρ^0 and $\rho^\pm$ percentages have both decreased by (5–7)%, but are still very large.

The channel designated as $\rho^0\rho^\pm\pi^\mp$ is exclusive of the channels $A_2^\pm\rho^\mp$ and $A_2^0\rho^0$, which both decay via $\rho^0\rho^\pm\pi^\mp$. It is interesting that the $\rho^0\rho^\pm\pi^\mp$ channel is of constant percentage, within errors, over the energy range, and that the $\rho^0\pi^+\pi^-\pi^0$ and $\rho^\pm\pi^+\pi^-\pi^\mp$ channels are everywhere consistent with zero. The $A_2^0\rho^0$ and $A_2^\pm\rho^\mp$ channels are larger at low energy, and hence account for the rise in $\rho^0\rho^\pm\pi^\mp$ at low energies seen in Fits (1), (2), and (3). The $A_2^0\pi^+\pi^-$ and $A_2^\pm\pi^\mp\pi^0$ channels increase as energy

increases, consistent with the increase in $\rho^0\pi^+\pi^-\pi^0$ and $\rho^\pm\pi^+\pi^-\pi^\mp$ with energy seen in the earlier fits.

From Table IV it is seen that the total χ^2 for 1671 bins has been reduced by 224 from Fit (3), down to 3261. As expected, the addition of the A_2 meson helped the fits of the mass spectra involving A_2's: $M(2\pi^\pm\pi^\mp)$, $M(\pi^+\pi^-\pi^0)$, $M(\pi^+\pi^-\pi^0)$ opposite a ρ^0, $M(\rho^0\pi^\pm)$, and $M(\rho^\pm\pi^\mp)$. Also improved were $M(2\pi^+2\pi^-)$ and $M(\pi^+\pi^-)$ opposite a $\rho^\pm$.

The addition of the $B^\pm$ mesons has not helped the χ^2 values of mass spectra involving ω^0 mesons. The mass spectra of $M(\omega^0\pi^\pm)$ fits less well with the B meson added, as does the $M(\pi^+\pi^-)$ opposite an ω^0. This should not be too alarming, however. The $B^\pm\pi^\mp$ and the $\omega^0\pi^+\pi^-$ are very aligned, or unphase-space-like systems. Since the likelihood function contains no information about this aligned behavior, Monte-Carlo-generated events weighted by the likelihood function should not be expected to reproduce the experimental data. Fortunately, most other channels are not as strikingly aligned, and hopefully this likelihood fitting is essentially correct.

5. *Summary of fit quality*

The data have been fitted with matrix elements for η^0, ρ^0, $\rho^\pm$, ω^0, f^0, g^0, A_2^0, $A_2^\pm$, and $B^\pm$-meson production and for correlation effects between pions of like charge. Comparison of the experimental spectra and the generated spectra shows that, though agreement is good in general, there are some systematic problems.

In the first place, there are the following problems with invariant mass predictions:

(i) $M(\pi^\pm\pi^\pm)$—see Fig. 5(a). The data are above the prediction in the lower mass (400–600 MeV/c^2) region and below in the higher (800–1500 MeV/c^2) region. Bose-Einstein correlations between pions of like charge could not entirely account for this effect.

(ii) $M(\pi^+\pi^-\pi^0)$—see Fig. 4(a). Though the shape of the experimental data plot is nearly the same as the plot of the generated data, the experimental plot appears shifted approximately 50 MeV/c^2 higher than the generated data plot. This effect is seen in the general $M(\pi^+\pi^-\pi^0)$ spectrum and in the more specialized plots: $M(\pi^+\pi^-\pi^0)$ opposite a ρ^0, $M(\rho^0\pi^0 \to \pi^+\pi^-\pi^0)$, and $M(\rho^\pm\pi^\mp \to \pi^+\pi^-\pi^0)$.

(iii) $M(2\pi^\pm\pi^\mp)$—see Fig. 4(b). Again, the shape of the experimental data plot is nearly the same as for the generated events; in this case, the plot of the experimental data appears shifted about 50 MeV/c^2 lower than the generated event spectrum. This effect is seen in the $M(2\pi^\pm\pi^\mp)$ plot and in the $M(\rho^0\pi^\pm \to 2\pi^\pm\pi^\mp)$ and $M(f^0\pi^\pm \to 2\pi^\pm\pi^\mp)$ spectra.

(iv) $M(2\pi^+2\pi^-)$—see Fig. 5(e). For this spectrum, the experimental data plot is peaked lower than the generated event plot.

Second, there are more specific problems with the $\omega^0\pi^+\pi^-$ system:

(i) $M(\pi^+\pi^-)$ opposite an ω^0—see Fig. 5(d). The fit in the ρ region is poor; the ρ appears much narrower than the 168 MeV/c^2 width used in the likelihood function. The generated events do not exhibit as deep a valley between the ρ^0 and f^0 peaks as the experimental data do. Also, the likelihood parameterization underestimates the number of events in the $M(\pi^+\pi^-)$ above about 1300 MeV/c^2.

(ii) $M(\pi^+\pi^-\pi^0)$ opposite the f^0 and opposite $M(\pi^+\pi^-)$ above 1320 MeV/c^2—see Fig. 5(f). The likelihood fit underestimates the number of ω^0 with $M(\pi^+\pi^-)$ in the f^0 and above regions.

(iii) the $B^\pm$ meson. As discussed earlier, the likelihood fit predicts about 2% $B^\pm\pi^\mp$ production, but this worsens the fit to the $M(\omega^0\pi^\pm)$ and $M(\pi^+\pi^-)$ opposite an ω^0 spectra.

It is not unreasonable that these problems exist, since the likelihood parameterization does not include any knowledge of the production mechanism. Indeed, the center-of-momentum angle between the antiproton (proton) and the negative (positive) pion [Fig. 6(a)] shows forward and backward peaking; for comparison Fig. 6(b) shows strong forward peaking in the center-of-momentum angle between like-sign pions. This introduces correlations into the angles between pions not included in the phase-space-like likelihood parametrization. Furthermore the χ^2 values in Table IV for $\pi^+\pi^+$ and $\pi^-\pi^-$ are quite different, probably indicating that the confidence-level cuts have introduced some non-charge-symmetric bias.

We should not overemphasize these disagreements. A great many of the projected effective-mass plots agree very well with the results of these fits. The results of Fit (4) are given in units of mb in Table X.

From the studies of this section it is clear that the percentages of resonance channels depend on both the parameterization formula and the parameter values. Before further discussing the fitting results, let us discuss the uncertainty inherent in any conclusions that might be drawn concerning resonance production.

Qualitatively, it is seen that general features, such as which channels dominate or the dependence of channel percentages on energy, are relatively independent of the parameterization used.

Quantitatively, the effect of uncertainties is much greater. The percentages for the total ρ^0, total $\rho^\pm$, $\rho^0\rho^\pm\pi^\mp$, $\rho^0\pi^+\pi^-\pi^0$, and $\rho^\pm\pi^+\pi^-\pi^\mp$ channels may vary by up to (5–10)% of the five-pion cross section, depending upon such factors as ρ width,

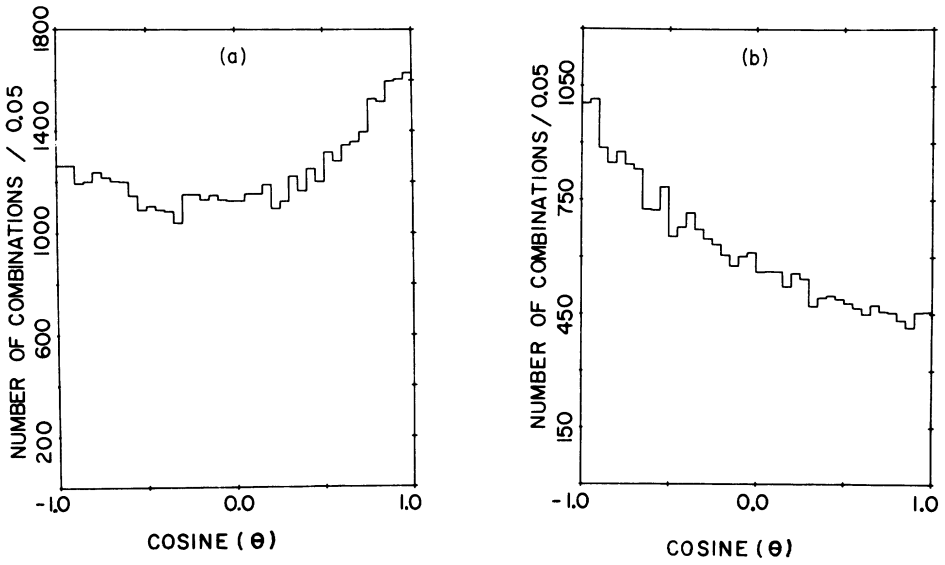

FIG. 6. c.m. angle distributions (all momenta). (a) $\bar{p}-\pi^-$ and $p-\pi^+$ (4 entries/event); (b) $\pi_1^+-\pi_2^+$ and $\pi_1^--\pi_2^-$ (2 entries/event).

inclusion or exclusion of certain meson channels (A_2, for example), or the Goldhaber effect, and so on. Note that, since the five-pion cross section is about 10 mb in this energy range, a (5–10)% uncertainty is, equivalently, a 0.5- to 1.0-mb uncertainty. On top of these systematic differences, one must add the statistical errors. Thus it is very difficult to compare one's data with the experimental data at other energies which, in most cases, have been analyzed with different procedures and parameterizations. Such a comparison showing no energy-dependent structure could be hiding a 0.5 to 1.0 mb enhancement, or, conversely, a 0.5 to 1.0 mb enhancement could be due to systematic differences in analysis.

Though in the case of ρ channels the systematic uncertainties appear to be of equal or greater importance than the statistical errors, the non-ρ channels—that is, the f^0, η^0, and ω^0 channels—appear to be more independent of systematic differences; the only errors to contend with are the relatively small statistical errors.

B. Discussion of results

1. *Results of this experiment*

The resonance-channel cross sections for the best maximum-likelihood fit to the data, Fit (4), are given in mb in Table X and as percentages of the five-pion cross section in Table IX.

It is immediately seen that the production of neutral and charged ρ mesons dominates the five-pion reaction. The neutral ρ and charged ρ cross sections are equal within errors, with a magnitude of nearly one-half the five-pion cross section. The ω^0 meson is also copiously produced, with a cross section of about 20% of the five-pion cross section. The f^0 meson is produced, but only in conjunction with the ω^0 or ρ mesons.

The largest channel is the $\rho^0\rho^\pm\pi^\mp$ channel, accounting for over one-third of the five-pion events, though the neutral mode of this channel, $\rho^0\rho^0\pi^0$, is at least an order of magnitude smaller. A similar situation exists in the $\rho f\pi$ channels: The charged mode $\rho^\pm f^0\pi^\mp$ accounts for over 6% of the five-pion events, whereas the neutral mode $\rho^0 f^0\pi^0$ is zero within our errors. Let us consider the isospin situation. The antiproton-proton system can be

TABLE X. Results of likelihood Fit (4) in units of mb.

Channel	Incident antiproton momentum (GeV/c) 1.77, 1.83, 1.88, 1.95	1.63	1.77	1.83	1.88	1.95	2.20
$\rho^0\pi^+\pi^-\pi^0$	0.00	0.02	0.00	0.00	0.00	0.00	0.00
$\rho^0\rho^\pm\pi^\mp$	2.63	3.46	2.52	2.70	3.02	1.97	1.85
$\rho^\pm\pi^+\pi^-\pi^\mp$	0.00	0.00	0.00	0.00	0.00	0.41	0.04
$\rho^0\rho^0\pi^0$	0.21	0.05	0.34	0.03	0.14	0.36	0.46
$\rho^0 f^0\pi^0$	0.13	0.32	0.00	0.28	0.14	0.21	0.00
$A_2^0\pi^+\pi^-$	0.49	0.18	0.51	0.23	0.48	0.61	0.45
$A_2^0\rho^0$	0.15	0.77	0.30	0.34	0.08	0.00	0.00
$A_2^\pm\pi^\mp\pi^0$	0.15	0.31	0.08	0.15	0.11	0.21	0.60
$A_2^\pm\rho^\mp$	0.37	0.01	0.58	0.34	0.18	0.38	0.04
$f^0\rho^\pm\pi^\mp$	0.50	0.34	0.78	0.53	0.34	0.27	0.73
$\omega^0\pi^+\pi^-$	0.73	1.06	0.63	0.73	0.95	0.56	0.62
$\omega^0\rho^0$	0.18	0.36	0.30	0.09	0.22	0.12	0.05
$\omega^0 f^0$	0.59	0.64	0.74	0.62	0.51	0.53	0.20
$B^\pm\pi^\mp$	0.18	0.38	0.08	0.28	0.11	0.25	0.26
$2\pi^+2\pi^-\pi^0$	2.62	2.69	2.57	2.71	2.46	2.65	1.67
All ρ^0	4.03	5.34	4.48	3.97	4.04	3.61	3.48
All $\rho^\pm$	4.14	4.78	4.70	4.17	4.12	3.64	3.12
All ω^0	1.68	2.43	1.76	1.71	1.79	1.46	1.13
All $\rho^0\rho^\pm\pi^\mp$	3.15	4.26	3.41	3.42	3.29	2.37	1.89
Five-pion cross section	8.97	10.63	9.28	9.05	8.76	8.69	7.03

in either an $I, I_z = 0, 0$ or $1, 0$ state, since the antiproton is a $\frac{1}{2}, -\frac{1}{2}$ state and the proton is a $\frac{1}{2}, \frac{1}{2}$ state. The $\rho^0\pi^0$ system can combine in a 0, 0 state or a 2, 0 state, since the ρ^0 and the π^0 are both 1, 0 particles. For the $\rho^0\rho^0\pi^0$ channel, isospin conservation implies that the additional ρ^0 combines with the $\rho^0\pi^0$ to form a 1, 0 state. Similarly, for the $\rho^0 f^0\pi^0$ channel, isospin conservation implies that the f^0, a 0, 0 state, combines with the $\rho^0\pi^0$ to form a 0, 0 state. Thus, since the $\rho^0\rho^0\pi^0$ must be an $I = 1$ system and the $\rho^0 f^0\pi^0$ must be an $I = 0$ system, the suppression of these channels cannot be explained as suppression of the cross section for one initial isospin state.

The A_2 meson, decaying via $\rho\pi$, is seen in the neutral and charged states, in the channels $A_2\pi\pi$ and $A_2\rho$. The $A_2\rho$ channel, decaying via $\rho^0\rho^\pm\pi^\mp$, is found primarily in the 1.63- to 1.95-GeV/c data, decreasing with energy. The $A_2\pi\pi$ channel appears to increase slowly with energy. The $\rho^0\rho^\pm\pi^\mp$ channel, exclusive of $A_2\rho$, is of constant percentage within errors over the energy range, as are all the ω^0 channels. The $B^\pm\pi^\mp$ channel, decaying via $\omega^0\pi^+\pi^-$, constitutes about 2% of the five-pion events over the entire energy range.

Note that qualitative features such as those presented above were found in sub section A to be relatively independent of the likelihood parameterization used.

2. *Comparison with other experiments*

In Sec. II B, it was seen that apparent inter-bubble-chamber normalization problems led to two different smoothly decreasing cross sections for the five-pion channel, approximately (10–20)% different in magnitude. Since there is no indication of significant structure in these five-pion cross sections, let us remove the normalization problem by considering resonance production only in terms of percentages of the five-pion cross section. The major uncertainties remaining are those resulting from the lack of an approach to resonance fitting which is consistent between experiments.

It was found that fluctuations in resonance percentages due to variation of resonance widths, exclusion or inclusion of resonances, or addition of Bose-Einstein correlations in the likelihood function can indeed be larger than the statistical errors. For several experiments below 2.5 GeV/c, resonance percentages were arrived at via fitting mass spectra or mass versus mass plots; the equivalence of these procedures and the maximum-likelihood method are not clear.

In Table XI the percentages of various resonance channels are presented.[4-6,8,13-16] The Michigan results presented here are from Fit (4) except that ωf and $\omega\rho$ percentages are taken from Fit (3).

Let us examine the total percentages of ρ^0, $\rho^\pm$, and ω^0 mesons produced, that is, the single resonance plus anything; these percentages are plotted in Fig. 7(a). $\rho\rho\pi$ events are counted twice in computing these percentages. Though the cross-section percentages of all three mesons are bumpier than statistically expected, smooth energy-dependent structures are suggested. The ω^0 cross-section percentage appears to rise a little, from the at-rest value of 24% to about 33%, but

TABLE XI. Resonance percentages in the 0.0- to 2.5-GeV/c $\bar{p}$ momentum range.

Experimenter (reference)	Antiproton momentum (GeV/c)	All ρ^0	All $\rho^\pm$	All ω^0	$\rho^0\rho^0\pi^0$	$\rho^0\rho^\pm\pi^\mp$	$\omega^0\rho^0$	$\omega^0 f^0$	$\omega^0 g^0$
Columbia (13)	0.0	39	34	20	...	...	4.0	...	...
France (14)	0.7	33	28	36	0.0	19	14.0	15.0	...
BNL (4,15)	1.1	38	36	25	0.0	35	2.6	7.0	...
Liverpool (16)	1.2	35	30	30	3.0	22	6.7	6.0	...
ANL (6)	1.22	45	47	34	4.0	27	5.3	9.6	...
ANL (6)	1.32	48	44	28	5.2	27	6.0	7.5	...
BNL (4,15)	1.33	37	43	23	5.5	25	2.7	5.5	...
ANL (6)	1.43	49	43	28	5.1	24	4.9	10.0	...
BNL (4,15)	1.53	44	52	19	0.0	35	3.3	4.5	...
ANL (6)	1.54	51	49	24	1.1	31	3.6	8.9	...
ANL (6)	1.62	43	43	24	0.0	25	2.0	12.0	...
Michigan	1.62	50	45	23	0.5	40	3.4	5.6	5.0
Michigan	1.76	47	49	19	3.6	36	3.2	7.9	3.0
Michigan	1.82	44	46	19	0.3	37	1.0	7.1	2.5
Michigan	1.88	46	47	20	1.6	37	2.5	6.2	2.7
Michigan	1.94	42	43	17	4.2	28	1.4	7.1	3.5
Michigan	2.20	50	44	16	6.6	27	0.8	3.3	1.8
ANL (5, 6)	2.3	44	45	16	3.1	18	2.8	3.7	2.0
Liverpool (8)	2.5	51	49	18	2.5	23	1.9	2.7	2.6

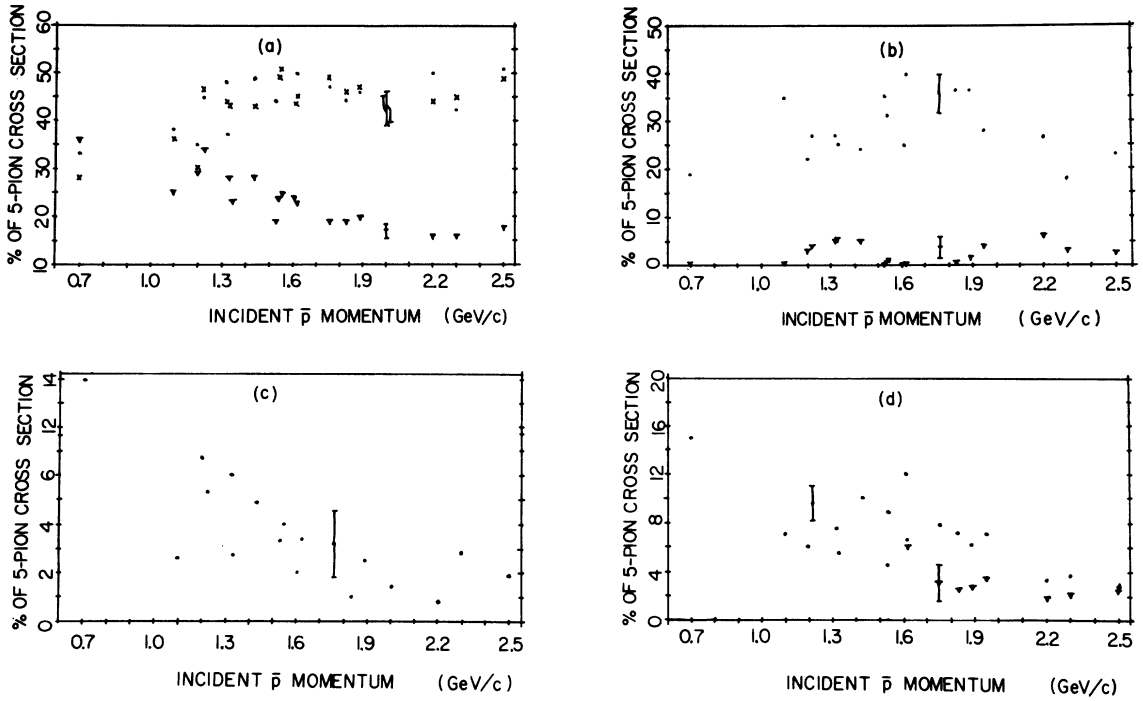

FIG. 7. Percentages of various channels as a function of incident momentum (typical error bars indicated). (a) Total ρ^0 (•), total $\rho^\pm$ (×) and total ω^0 (▼) percentages; (b) $\rho^0\rho^0\pi^0$ (▼) and $\rho^0\rho^\pm\pi^\mp$ (•) percentages; (c) $\omega^0\rho^0$ percentages; (d) $\omega^0 f^0$ (•) and $\omega^0 g^0$ (▼) percentages.

declines slowly at momenta above 1.2 GeV/c. The ρ^0 and $\rho^\pm$ percentages are approximately constant from 1.2 GeV/c to 2.5 GeV/c, and the two percentages appear to be equal in magnitude, within errors.

From this point on, the results become less clear. Consider the channels $\rho^0\rho^0\pi^0$ and $\rho^0\rho^\pm\pi^\mp$. In these cases, two distinct pairs of pions form ρ mesons. Unfortunately, the ρ meson is a wide meson, and two-pion phase space is peaked near the ρ region; many phase-space events "look like" $\rho\rho\pi$ events, and determining the exact amount of $\rho\rho\pi$ is difficult. The amount of $\rho\rho\pi$, $\rho^0\rho^\pm\pi^\mp$ in particular, is very dependent on the ρ width chosen and on the inclusion or exclusion of the Goldhaber effect [compare Fits (2) and (3)]. Another confusing problem is that of resonances which decay via $\rho\pi$ or $\rho\rho$ and contribute to the $\rho\rho\pi$ channels. At 1.2 GeV/c, Donald *et al.*[16] report the observation of either a $\rho\pi$ enhancement at 1080 MeV/c^2, possibly the A_1, or a $\rho^0\rho^0$ enhancement at 1400 MeV/c^2, possibly the $\rho\rho(1400)$. Some A_2 production is seen in the 1.2–1.5 GeV/c range. Unfortunately, neither the A_1 nor the $\rho\rho(1400)$ are established elsewhere in $\bar{p}p$ interactions. Our experiment finds little, if any, A_1 production, but significant A_2 production from 1.63 to 2.2 GeV/c, including sizable $A_2\rho$ decaying via $\rho^0\rho^\pm\pi^\mp$ from 1.63 to 1.95 GeV/c. Clayton *et al.*[8] report $A_2\pi\pi$ production, but no $A_2\rho$ production, at 2.5 GeV/c, in agreement with our 2.2 GeV/c data; Clayton also reports $A_3^\pm\rho^\mp$ decaying via $\rho^0\rho^\pm\pi^\mp$. The primary decay mode of the A_3 meson was believed to be $f^0\pi^\pm$, not $\rho^0\pi^\pm$, but Clayton sees no A_3 decaying via $f\pi$.

With these problems in mind, let us look at the experimental percentages of the $\rho^0\rho^0\pi^0$ and $\rho^0\rho^\pm\pi^\mp$ channels, shown in Fig. 7(b). The dominance of the $\rho^0\rho^\pm\pi^\mp$ is most obvious. With $A_2\rho$ and $A_3\rho$ channels included, as in Fig. 7(b) and Table XI, the $\rho^0\rho^\pm\pi^\mp$ percentages in these data and the 2.5-GeV/c data of Clayton appear higher than in other experiments. This effect could be due to the emergence of the $A_2\rho$ and $A_3\rho$ channels, or due merely to different fitting techniques. The $\rho^0\rho^0\pi^0$ channel appears to show an enhancement in the 1.2- to 1.4-GeV/c region, the location of the $T(2190)$ enhancement observed in $\bar{p}p$ interactions. The significance is increased by the fact that three different research groups show the $\rho^0\rho^0\pi^0$ production in this region, and four groups show no production in the regions above or below. But, considering the 1.1- to 1.6-GeV/c region, it is seen that there is a dip in the $\rho^0\rho^\pm\pi^\mp$ channel of similar magnitude to the enhancement in the $\rho^0\rho^0\pi^0$ channel. Due to the many problems concerned with these channels, it is difficult to draw con-

clusions.

Due to the distinguishability of the ω^0 meson and the relative stability of the ω^0-channel percentages in this analysis, one might expect the comparison of ω^0 channels to show less experiment to experiment variation. Examination of Table XI and Fig. 7(c) shows that the percentage of $\omega^0\rho^0$ is relatively consistent, decreasing slowly above 1.2 GeV/c, in the same manner as the total ω^0 percentage. From at-rest to 2.5-GeV/c incident momentum, the maximum invariant mass of the $\pi^+\pi^-$ pair opposite the ω^0 meson increases from 1100 MeV/c^2 to 1800 MeV/c^2, and, as energy increases, the emergence of the $\omega^0 f^0$ and $\omega^0 g^0$ channels is seen. Contrary to expectations, inter-experimental fluctuations in these channels [see Fig. 7(d)] are in many cases much larger than the reported statistical errors. The most likely explanation of these fluctuations is the difficulty in determining the production of a resonance (the f^0 or g^0), which is partially suppressed by phase-space considerations and whose background is confused by the production alignment of the $\omega^0\pi^+\pi^-$ system which appears to enhance the high $\pi^+\pi^-$ masses.

Thus it appears that the total ρ^0, total $\rho^\pm$, and total ω^0 percentages exhibit smooth structure as a function of the incident $\bar{p}$ momentum, and that the $\rho^0\rho^\pm\pi^\mp$ channel dominates throughout the low energies. There may be an enhancement in the $\rho^0\rho^0\pi^0$ channel in the $T(2190)$ region; no other evidence for direct-channel resonances is seen.

V. CONCLUSIONS

In Sec. II, it was seen that the five-pion cross section fell from 10.6 to 7.05 mb over the incident antiproton momentum range of 1.62 to 2.20 GeV/c. The cross sections of this report compare well with the five-pion cross sections at other energies in the range of 1.1 to 2.9 GeV/c. Though, due to an apparent normalization difference, the cross sections from experiments run in the Brookhaven National Laboratory's 31-in. bubble chamber were about (10–15)% lower than the cross sections from experiments run in the Argonne National Laboratory's and CERN's bubble chambers, no sizable five-pion cross section enhancements were indicated. The final sample of five-pion events for this report consisted of 12 357 events spread nearly evenly over the six momenta, with an estimated contamination of only 1%.

The properties of mesons observed in the five-pion channel were discussed in Sec. III. Fits to the dipion mass spectra in the ρ region with six different Breit-Wigner functions found that both the ρ^0 and $\rho^\pm$ mesons were best represented by the simplest Breit-Wigner function attempted, with constant width Γ. The mass of the ω^0 and η^0 mesons agreed well with the documented values. An $\omega^0\pi^\pm$ mass enhancement consistent with the mass of the B meson was seen, though the large background prevented further analysis. The invariant mass spectra also indicated f^0, g^0, and $A_2^\pm$ meson production, though again the backgrounds were too large to allow analysis of the resonance properties.

The percentages of resonance channels were examined in Sec. IV by the maximum-likelihood method. Using likelihood amplitudes based on Breit-Wigner functions and meson-decay matrix elements, it was found that the five-pion channel is dominated by the production of ρ and ω mesons. The total cross sections for ρ^0 and $\rho^\pm$ are both on the order of one-half of the five-pion cross section; the total ω^0 cross section is about 20% of the five-pion cross section. The dominant channel is $\rho^0\rho^\pm\pi^\mp$, which accounts for (35–45)% of the five-pion events over the 1.63 to 2.20 GeV/c incident $\bar{p}$ momentum range. The f^0 meson is produced only in conjunction with the ω and ρ mesons. The $A_2\pi\pi$ channel, decaying via $\rho\pi\pi\pi$, appears to increase slightly with energy, whereas the $A_2\rho$ channel, decaying via $\rho^0\rho^\pm\pi^\mp$, decreases with energy. The percentage of $\rho^0\rho^\pm\pi^\mp$ exclusive of the $A_2\rho$ channels is constant over these energies. The $B^\pm\pi^\mp$ channel, decaying via $\omega^0\pi^+\pi^-$, accounts for only about 2% of the five-pion cross section.

It was found that the charged modes $\rho^0\rho^\pm\pi^\mp$ and $f^0\rho^\pm\pi^\mp$ have cross sections over an order of magnitude larger than the neutral modes $\rho^0\rho^0\pi^0$ and $f^0\rho^0\pi^0$. The suppression of the neutral channels could not be explained in terms of suppression of a single isospin state.

Though the magnitude of the log likelihood indicated a good likelihood parameterization, comparison of the experimental and Monte-Carlo-generated invariant mass spectra indicated certain systematic differences. These differences were not too unexpected, since no production mechanisms were employed in the likelihood function for resonance processes, and angular distributions indicated non-phase-space-like alignments.

In order to test the stability of the resonance percentages, a different Breit-Wigner function for the ρ was tried, the Breit-Wigner ρ width was varied, resonance amplitudes were added coherently, and the strength of the Goldhaber effect was varied. It was found that the variation of the ρ channel percentages for these parameterization changes was in many cases larger than the statistical errors; the total ρ^0 percentage, the total $\rho^\pm$

percentage, and the $\rho^0\rho^\pm\pi^\mp$ percentage changed by up to (8–10)% of the five-pion cross section. The ω^0 channels were relatively unaffected by these changes. In comparing resonance percentages between experiments, it was found that fluctuations between experiments were indeed larger than statistically expected, probably due to the different methods employed in determining the resonance percentages.

ACKNOWLEDGMENTS

We wish to thank Professor C. T. Murphy for his assistance in the earlier aspects of this experiment. We are also indebted to Dr. F. Schweingruber, Dr. L. Voyvodic, and the crew of the 30-in. bubble chamber. Finally, we thank the scanning, measuring, and programming staff associated with this study.

---

*This work was supported by the U. S. Atomic Energy Commission.

†Present address: U. S. Naval Academy, Computer Science Department, Annapolis, Maryland.

‡Present address: Flat 4, 221 Avoco St., Randwick, N. S. W. 2031, Australia.

[1]J. Davidson, J. W. Chapman, R. W. Green, J. Lys, and B. P. Roe, preceding paper, Phys. Rev. D 9, 77 (1974).

[2]J. W. Chapman, J. Davidson, R. Green, J. Lys, B. Roe, and J. C. Vander Velde, Nucl. Phys. B24, 445 (1970).

[3]J. Davidson, thesis, University of Michigan, 1972 (unpublished).

[4]G. Kalbfleisch, R. Strand, V. Vanderberg, Phys. Lett. 29B, 259 (1969).

[5]T. W. A. Cooper, Fields, D. S. Rhines, and W. W. M. Allison, Phys. Rev. Lett. 27, 1749 (1971).

[6]D. Rhines, private communication (1971).

[7]D. Parker, private communication (1971).

[8]J. Clayton, P. Mason, H. Muirhead, K. Whiteley, R. Rigopoulos, P. Tsilimigras, and A. Vayaki-Serafimidou, Nucl. Phys. B30, 605 (1971).

[9]R. J. Abrams, R. L. Cool, G. Giacomelli, T. F. Kycia, B. A. Leontić, K. K. Li, and D. N. Michael, Phys. Rev. Lett. 18, 1209 (1967).

[10]Particle Data Group, Rev. Mod. Phys. 43, S1 (1971).

[11]C. Baltay, J. C. Severiens, N. Yeh, and D. Zanello, Phys. Rev. Lett. 18, 93 (1967).

[12]G. Goldhaber, S. Goldhaber, W. Lee, and A. Pais, Phys. Rev. 120, 300 (1960).

[13]C. Baltay, P. Franzini, G. Lütjens, J. C. Severiens, D. Tycko, and D. Zanello, Phys. Rev. 145, 1103 (1966).

[14]Lab. de Phys. Nucl. Collège de France, paper No. 241, *Proceedings of the Fifth Lund International Conference on Elementary Particles, Lund, 1969,* edited by G. von Dardel (Berlingska, Boktryckeriet, Lund, Sweden, 1970).

[15]G. Kalbfleisch, private communication (1971).

[16]G. Donald, G. N. Edwards, R. S. Moore, E. J. C. Read, S. Reucroft, T. Buran, A. G. Frodesen, S. Sire, P. Saetre, A. Bettini, S. Limentani, L. Peruzzo, R. Santangelo, and S. Sartori, Nucl. Phys. B11, 551 (1969).